

# Thermodynamic and Kinetic Limitations for Peroxide and Superoxide Formation in Na-O2 Batteries

**Mekonnen, Yedilfana S.; Christensen, Rune; García-Lastra, Juan M.; Vegge, Tejs**

*Published in:*
Journal of Physical Chemistry Letters

*Link to article, DOI:*
10.1021/acs.jpclett.8b01790

*Publication date:*
2018

*Document Version*
Peer reviewed version

# Thermodynamic and Kinetic Limitations for Peroxide and Superoxide Formation in Na–$O_2$ Batteries

Yedilfana S. Mekonnen[1,2], Rune Christensen[1], Juan M. Garcia-Lastra[1], Tejs Vegge[1*]

[1]Department of Energy Storage, Technical University of Denmark, Fysikvej, Building 309, 2800 Kgs Lyngby, Denmark

[2]Center for Environmental Science, College of Natural and Computational Sciences, Addis Ababa University, P. O. Box 1176, Addis Ababa, Ethiopia

[*]Corresponding Author E-mail: teve@dtu.dk

## Abstract

The Na–$O_2$ system holds great potential as a low cost, high energy density battery, but under normal operating conditions, the discharge is limited to sodium superoxide ($NaO_2$), whereas the high capacity peroxide state ($Na_2O_2$) remains elusive. Here, we apply density functional theory calculations with an improved error-correction scheme to determine equilibrium potentials and free energies as a function of temperature for the different phases of $NaO_2$ and $Na_2O_2$, identifying $NaO_2$ as the thermodynamically preferred discharge product up to ~120 K, after which $Na_2O_2$ is thermodynamically preferred. We also investigate the reaction mechanisms and resulting electrochemical overpotentials on stepped surfaces of the $NaO_2$ and $Na_2O_2$ systems, showing low overpotentials for $NaO_2$ formation ($\eta_{\mathrm{dis}} = 0.14$ V) and depletion ($\eta_{\mathrm{cha}} = 0.19$ V), whereas the overpotentials for $Na_2O_2$ formation ($\eta_{\mathrm{dis}} = 0.69$ V) and depletion ($\eta_{\mathrm{cha}} = 0.68$ V) are found to be prohibitively high. These findings are in good agreement with experimental data on the thermodynamic properties of the $Na_xO_2$ species and provide a kinetic explanation for why $NaO_2$ is the main discharge product in Na–$O_2$ batteries under normal operating conditions.

**Key Words:** Na–$O_2$ batteries, $NaO_2$, $Na_2O_2$, DFT, Thermodynamic and Kinetic, Overpotentials

## Possible Electrochemical Discharge Products in Na-$O_2$ Batteries

$Na_2O_2$

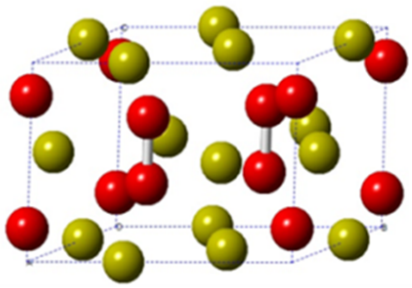

$\Delta G$ = -2.4 eV

$\eta_{dis}$ = 0.69 eV

Thermodynamically favored

Kinetically favored

$NaO_2$

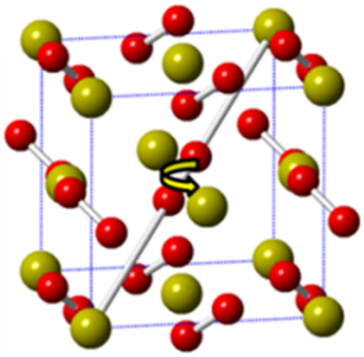

$\Delta G$ =-2.3 eV

$\eta_{dis}$ = 0.14 eV

# I. Introduction

In the last decade, significant efforts have been paid to the development of next generation battery technologies. In particular metal–air batteries (e.g. Li–, Na–, Mg–, Al–, Fe– and Zn–$O_2$ batteries) in either aqueous or non-aqueous (aprotic) electrolytes have gained significant attention, especially for its possible use in electric vehicles. The cost of commercially available Li–ion batteries is generally too high and the energy storage capacity is too low to solve the increasing demands on batteries for sustainable transportation. [1] Metal–air batteries have high theoretical specific energies since the technology, once mature, would apply metal as the anode and oxygen gas from air on the cathode side. The discharge products are generally peroxides and/or superoxides, depending on the experimental conditions and cell components used in the system. The oxygen reduction (ORR) and oxygen evolution reaction (OER) are the two main reactions taking place reversibly during discharge and charge, respectively. However, metal–air battery technologies are limited by a number of drawbacks and challenges, which must be resolved before becoming commercially viable, i.e., low accessible capacity (sudden death) [2], poor electronic conductivity and rechargeability [3,4] limited chemical and electrochemical stability of electrodes [5,6] electrolytes [7], salts [8], and high sensitivity to air impurities such as water and $CO_2$. [9–11]

Among the rechargeable metal-oxygen battery systems reported so far, the Li–$O_2$ couple offers higher equilibrium potential (~2.96 V) and specific capacity (~3,842 mAh/g), which is comparable to the gravimetric energy density of gasoline [12] and nearly an order of magnitude higher than current Li–ion batteries. [13] However, in practice, non-aqueous Li–$O_2$ batteries suffer from poor rechargeability and high overpotentials, particularly for the charging process. [14], [15] Although the capacity and equilibrium potential are lower, the Na–$O_2$ battery system displays certain advantages over the Li–$O_2$ battery and similar batteries. The non-aqueous secondary Na–$O_2$ battery operates at low dis/charge overpotentials (< 200 mV) even at higher current densities (0.2 mA/cm$^2$) and yields high electrical energy efficiency (90 %), which can be observed over multiple cycles. [16–20] The theoretical specific capacity of the Na–$O_2$ battery is ~1,500 mAh/g [18], when $NaO_2$ is deposited on carbon nanotubes. If, however, the peroxide, $Na_2O_2$, could be formed reversibly as for Li–$O_2$, it would be possible to increase the specific capacity to ~2,800 mAh/g. [21]

Hartmann *et al*. [17,22], McCloskey *et al*. [23] and Tarascon *et al.* [24] have reported sodium superoxide ($NaO_2$) as the dominant reaction product. Whereas, Kim *et al.* [21], Li *et al*. [25], Lie *et al*. [26] and Hu *et al*. [27] have reported sodium peroxide ($Na_2O_2$) as the dominant discharge product. Poor rechargeability (< 10 cycles) and high charging overpotential (> 1.3 V) is exhibited when $Na_2O_2$ is formed at the cathode at room temperature, which are similar to the drawbacks observed in the

Li–$O_2$ system. However, sufficiently lower dis/charge overpotentials and higher rechargeability are observed when $NaO_2$ is formed [17,18,20] Moreover, it has been also argued on the basis of density functional theory (DFT) calculations that the reason for $NaO_2$ formation over $Na_2O_2$ could be its conduction mechanism [28], solvents [29] and the presence of proton sources like water. [30]
Scanning electron microscopy (SEM) images have revealed that highly ordered cubic $NaO_2$ particles are grown at the carbon cathode surface. [17,22] A computational study by Kang *et al.* reports that $NaO_2$ is more stable at the nanoscale level (up to about 5 nm), whereas bulk $Na_2O_2$ is thermodynamically stable at standard conditions (in agreement with experimental observations). For electrochemical growth during battery discharge, the size of the $NaO_2$ particles is, however, found in the micrometer range (1-50 μm). [17] The observed stoichiometry of the particles can therefore not be explained solely from the effect of the differences in surface energy, nor the effect of e.g. increased oxygen partial pressure or temperature, which may lead to the formation of somewhat larger $NaO_2$ particles (up to 20 nm based on the calculations by Kang *et al*. [31]). This is further supported by the reported effect of the discharge rate on the sizes and distribution of $NaO_2$ on carbon nanotubes, where relatively small sizes (~50–500 nm) with a wide distribution are observed at low rate and large sizes (~2 μm) with a narrow distribution are observed at higher rates. [32]

Regarding the $NaO_2$ charge/discharge mechanism, Hartmann *et al.* have reported computational and experimental work, which indicates that large amounts of $NaO_2$ can be formed at the cathode. This is due to high solubility of $NaO_2$ in the liquid electrolyte, i.e. forming superoxide ions ($O_2^-$), followed by precipitation in the presence of sodium ions to form solid sodium superoxide. Therefore, the discharge mechanism may also follow a solution-precipitation mechanism in addition to the direct electrochemical growth of $NaO_2$ investigated here. [24,33]

The reaction for non-aqueous Na–$O_2$ cathode electrochemistry using ether based electrolytes like diglyme, is shown below. [23]

$$Na^+ + e^- + O_2 \leftrightarrow NaO_2, \qquad E^o = 2.27\ V\ vs.\ Na/Na^+$$

Here, we apply DFT calculations to investigate the thermodynamic and kinetic properties of the materials and reactions in Na–$O_2$ batteries. We will discuss the thermodynamic stability and kinetic overpotentials for the growth/depletion pathways of $NaO_2$ and $Na_2O_2$ on selected stepped model surfaces, i.e. (001) for $NaO_2$ and $(1\bar{1}00)$ for $Na_2O_2$ and the equilibrium potential of different phases of bulk $NaO_2$ and $Na_2O_2$ as a function of temperature. The stepped surfaces are likely to give accessible barriers and favorable nucleation sites for the minimum overpotential mechanism, as it has been reported in case of Li–$O_2$. [34]

It should be noted that the correct description of the thermodynamics of reactions involving superoxide vs. peroxide species (i.e. to describe the relative stability of $NaO_2$ vs. $Na_2O_2$ at finite temperatures) is computationally challenging, mainly due to the precession of misaligned superoxide species in the high temperature pyrite phase of $NaO_2$ (Fm3m above 231 K) relative to the low temperature pyrite phase ($Pa\bar{3}$, between 200 K and 231 K) (see Figure 1). Such effects and energetics are generally not accounted for in standard density functional theory (DFT) calculations, making it highly challenging to calculate the stability at finite temperatures. Systematic work on the modeling of alkali superoxides and peroxides using DFT+U and hybrid functional calculations is currently ongoing, but in the following, we describe a comparatively simple GGA-level computational approach using metal chloride reference energies [35], which yields excellent agreement with the experimental observations.

## II. COMPUTATIONAL METHODOLOGY

Calculations are performed using the PBE (Perdew-Burke-Ernzerhof) [36] exchange correlation functional as implemented in the GPAW package [37] using the Atomic Simulation Environment (ASE). [38] A real space grid basis set on the projector augmented wave (PAW) function method with frozen core approximation has been used with 0.18 Å grid point spacing. [39,40] Dipole corrections have been applied in the direction perpendicular to the slab surface and ionic optimization converged to a maximum residual force of 0.03 eV/Å. The $NaO_2$ growth/depletion mechanism is studied on the stepped (001) surface of $NaO_2$ in the $Pa\bar{3}$ space group, thus neglecting the precession of the superoxide ions. We have used the ferromagnetic phase of $NaO_2$ in all the calculations (i.e., the initial magnetic moment value of each O atom in $NaO_2$ was set to 0.5 since previous theoretical studies reported it to be more stable than the antiferromagnetic phase by 15 meV per formula unit. [28] The k-points are sampled with a $2 \times 4 \times 1$ Monkhorst-Pack mesh and the supercell consists of 60-72 atoms. A vacuum layer of 21.2 Å is used. A stepped $(1\bar{1}00)$ surface of $Na_2O_2$ (space group $P\bar{6}2m$) with a super cell consisting of 88-96 atoms slab with a 20 Å vacuum layer is used to study the $Na_2O_2$ growth/depletion mechanisms. This surface termination has been extensively studied in pristine form as well as in the presence of defects like steps and kinks for Li–$O_2$. [9,34,41–43] The k-points are sampled with a $2 \times 2 \times 1$ Monkhorst-Pack mesh.

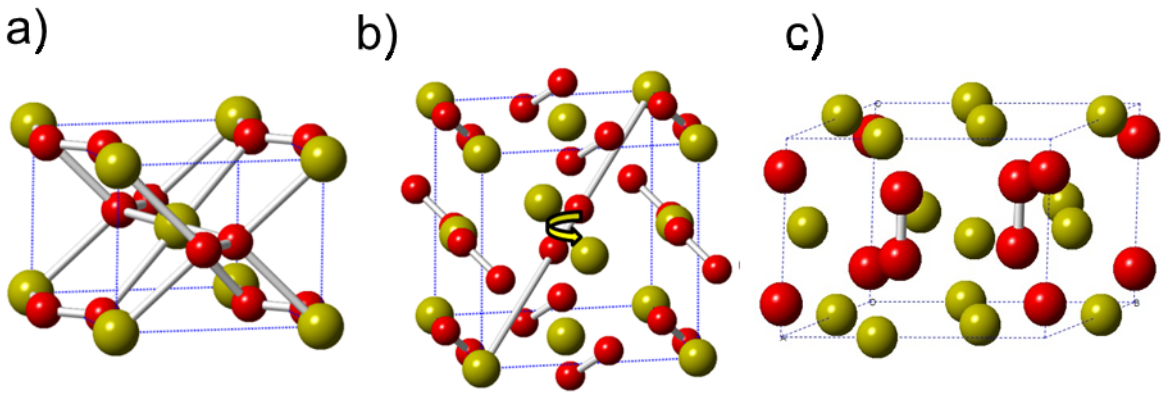


Figure 1: a) *Pnnm* $NaO_2$ orthorhombic structure (Marcasite) with lattice constants a = 4.26 Å, b = 5.44 Å, c = 3.36 Å. b) Face-centered cubic $\mathbf{Pa\bar{3}}$ $NaO_2$ structure (Pyrite) with lattice constant a = 5.523 Å. This phase occurs between 200 K and 231 K. Above 231 K the superoxide ions hop freely between the eight equivalent (111) orientations in a cube. Thus, the space group becomes Fm3m above 231 K. c) Hexagonal $Na_2O_2$ structure space group of $\mathbf{P\bar{6}_2m}$ with lattice constants of a = 6.39 Å, b = 6.39 Å and c = 4.6 Å. Color: Yellow (Sodium), Red (Oxygen).

The computational sodium electrode approach is used in the free energy calculations, analogous to the lithium electrode approach used for Li–air batteries. [44,45] At zero potential, U = 0, the bulk Na anode and Na ions in solution are assumed to be in equilibrium ($Na \leftrightarrow Na^+ + e^-$). The free energy change of the reaction is shifted by –neU at an applied bias, where n is the number of electrons transferred.

At neutral bias, all reaction steps are downhill in free energy, but at a given potential, the free energy difference changes for each step calculated as,

$$\Delta G_{i,U} = \Delta G_i - eU \quad (1)$$

The limiting discharge potential ($U_{discharge}$) is the lowest free energy step, $\Delta G_{i,min}$, along the reaction path, as this the first step to becomes uphill at a given potential. Likewise, the largest free energy step, $\Delta G_{i,max,}$ that is last to become downhill for the reverse charging reaction giving the limited charge potential ($U_{charge}$):

$$U_{discharge} = \min[-\Delta G_i/e] \text{ and } U_{charge} = \max[-\Delta G_i/e] \quad (2)$$

The calculated effective equilibrium potential can be obtained as $U_o = \Delta G/ne$.

Large systematic errors in the DFT description of superoxides, peroxides and monoxides have previously been documented by various groups and accounted for in various ways. [31,34,35] Here, we

adopt the recent approach of Christensen *et al*. [35] using NaCl as an indirect reference for sodium in order to better account for the oxidation state of Na in the Na–$O_2$ system. In line with Christensen *et al*. [35] an energy correction is applied to $O_2$ (g), which is notoriously difficult to describe correctly with DFT. With the computational approach used here, the optimal energy correction of $O_2$ (g) is –0.33 eV. The approach is chosen as it reduces the systematic errors significantly, while allowing consistent calculation of surfaces with oxide species in different oxidation states required for studying reactions in Na–$O_2$ batteries.

# III. RESULTS AND DISCUSSIONS

## 3.1. Enthalpy of Formation and Equilibrium Potential

To evaluate the accuracy of the calculations, bulk enthalpies of formation are compared with experiments [46] as seen in Table 1. The calculated formation enthalpies are converted to free energies at standard conditions ($\Delta H_{form} \rightarrow \Delta G_{form}$) using experimental entropies [46] and the equilibrium potentials are then calculated. As an alternative to using the experimental entropies, we also determine the equilibrium potentials using the simple approximation that the entropy can be described without explicitly considering the vibrational contributions to the entropy, as they are similar in $O_2$ (g) and the $O_2^-$ and $O_2^{2-}$ ions. As the superoxide ions are known to rotate easily in the $NaO_2$ pyrite phase at room temperature, the rotational degrees of freedom will to a good approximation also be similar for $O_2$ (g) and the superoxide ions. This is not the case for $Na_2O_2$, where the orientation of peroxide ions is well-defined at all relevant temperatures. This simple approximation has obvious flaws, e.g. will it not be able to capture the low temperature structural changes of $NaO_2$ due to differences in the rotational degrees of freedom of superoxide ions in different phases. It does, however, have the advantage of being simple to calculate with standard thermodynamic approaches. Comparison with experiment also proves the simple assumption to be reasonable (see Figure 2). It can also be seen that the experimental data for $NaO_2$ at 0 K is identical to the calculated result for the low temperature *Pnnm* structure.

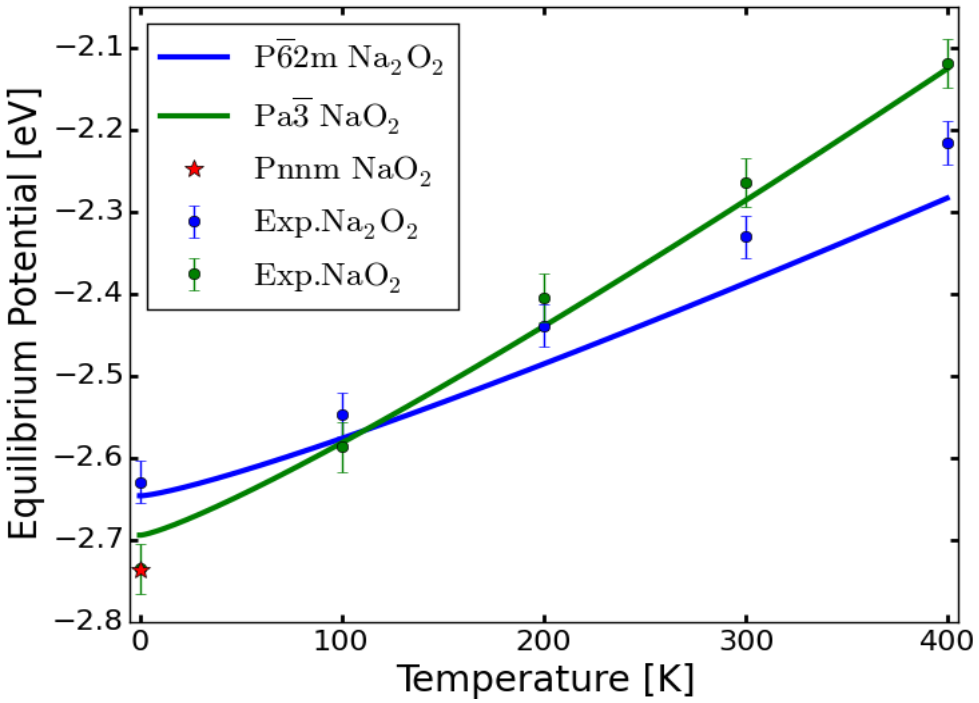


Figure 2: DFT-based equilibrium potentials predicted with the approximation that the temperature dependence is only due to the translational and rotational degrees of freedom for $O_2$ (g). This simple approximation is in good agreement with experimental data and reproduces relatively small free energy differences between $Na_2O_2$ and $NaO_2$.

For computational investigations of the electronic properties of $Na_xO_2$ species, e.g. band gaps and transport properties, standard GGA-level calculations are unable to capture the strongly correlated nature of $NaO_2$. [28] In the present work, however, the main focus is on the calculated formational enthalpies and here, the applied GGA-based approach agrees very well with both higher level methods [28] and experiments. [46] As seen in Table 1, the difference in equilibrium potential for $NaO_2$ and $Na_2O_2$ at standard conditions is less than 0.1 V for the experimental results, the calculated enthalpies with experimental entropies, and the purely theoretical calculations with approximated entropies. This indicates that required overpotentials in the electrochemical reactions to $Na_2O_2$ and $NaO_2$ could be decisive for the product selectivity.

Table 1: Calculations for $Na_2O_2$ and the pyrite phase of $NaO_2$ are compared with experimental values [46] in parentheses. Equilibrium potentials are calculated both using experimental entropies ($U_{0,\ exp\ \Delta S}$) and with a simple approximation to temperature dependence ($U_{0,\ approx.\ \Delta S}$).

| | $\Delta_f H°$ [eV] ($\Delta_f H°_{exp}$) | $U_{0,\ exp.\ \Delta S}$ [V] ($U_{0,\ exp}$) | $U_{0,\ approx.\ \Delta S}$ [V] |
|---|---|---|---|
| $\boldsymbol{Pa\bar{3}}$ $NaO_2$ | -2.74 (-2.71) | -2.30 (-2.27) | -2.29 |
| $\boldsymbol{P\bar{6}2m}$ $Na_2O_2$ | -5.29 (-5.32) | -2.32 (-2.33) | -2.39 |

### 3.2. $NaO_2$ Growth/Depletion Mechanisms on Stepped Surfaces

The thermochemical properties of the four steps in the $NaO_2$ growth/depletion are investigated on a stepped $(001)$ $NaO_2$ surface. The method does not include specific effects of the electrolyte or possible kinetic barriers associated with the transport of the ions/molecules. DFT calculations can determine the preferred pathways for the discharge/charge mechanisms by comparing the free energies of the adsorbed species at every single step. The stepped surface is constructed from the bulk crystal in a specific direction in such a way that four sodium superoxide species are added (removed) at the step site for the complete pathways of growth (depletion).

In general, the $NaO_2$ growth/depletion mechanisms on stepped (001) $NaO_2$ surface follows a four-step mechanism; each step involving the deposition (depletion) of either Na* or $NaO_2$* species (electrochemical steps) or $O_2$ species (chemical step) and both are taken into account to generate all likely pathways. The thermodynamically favorable path, i.e. the lowest overpotential path is selected. Thus, as shown in Figure 3, the first step for the (001) surface is the adsorption of $NaO_2$ at the bottom left site. This is the potential limiting step for discharge (-2.20 V) and is followed by adsorption of the second $NaO_2$ species at the bottom right site with a binding energy of -2.42 eV; the third and the fourth $NaO_2$ species are adsorbed by -2.22 eV and -2.54 eV, respectively. The fourth step is the limiting charge potential step and the growth mechanism is completed by forming 4 sodium superoxide species with equilibrium potential of -2.34 eV. The charging or desorption process follows the same reaction steps applied in reverse order (right to left), as shown in Figure 3 and Figure 4.

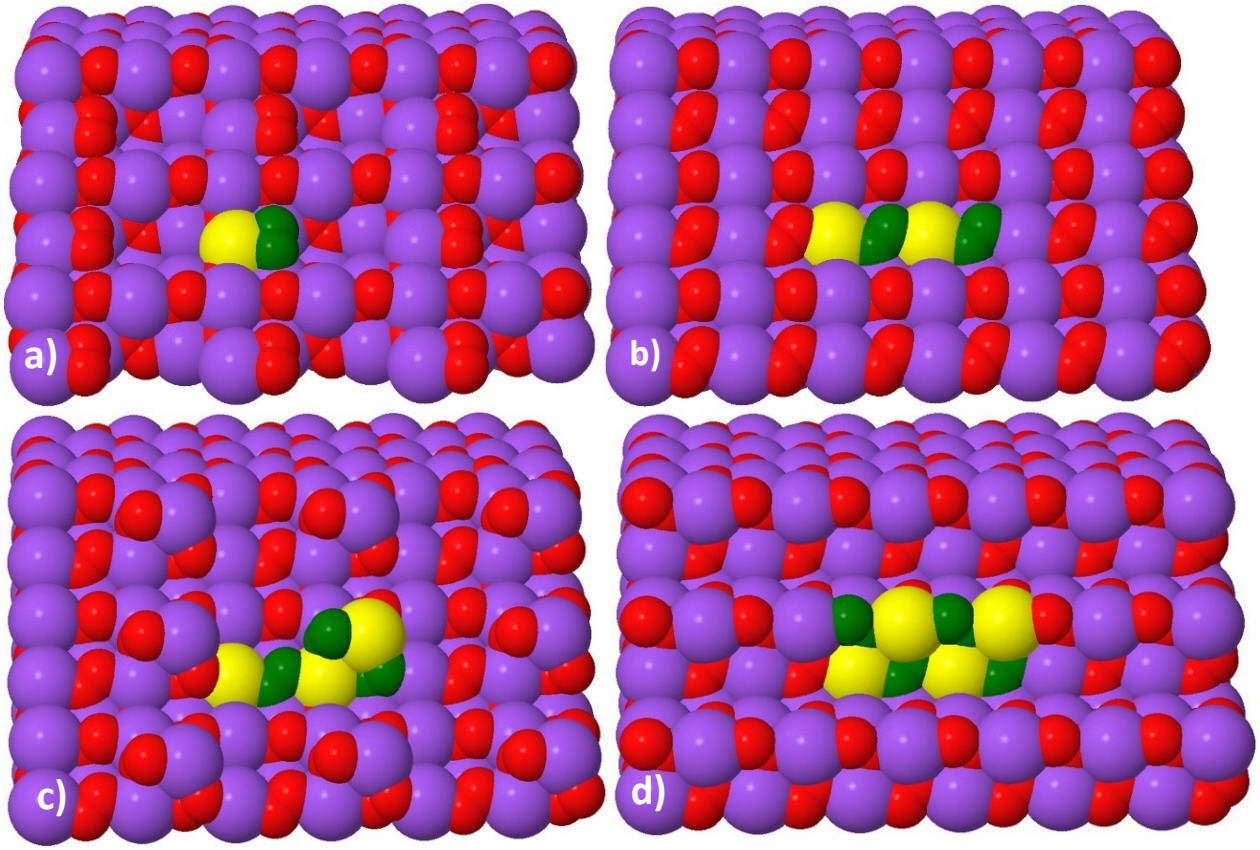


Figure 3: A four-step growth/desorption mechanism on the (001) step surface of $NaO_2$. In a) and b) $NaO_2$ species adsorbs to the bottom site. In c) and d) $NaO_2$ adsorbs to the top site to complete the 4 formula units $NaO_2$ reaction mechanism. Color: Na (purple) and O (red). Highlighted deposited ions: Na (yellow) and O (green).

The studies of the growth/depletion mechanisms on the stepped $NaO_2$ surface revealed that the fundamental overpotentials for both charge and discharge are very low, which has also been observed experimentally. [23] A discharge (charge) overpotential of $\eta_{dis} = 0.14$ V ($\eta_{cha} = 0.19$ V) for the growth (depletion) mechanism is observed. The calculated equilibrium potential at the surface ($U_{o,surf}$ 2.34 V) is marginally higher than the calculated bulk value of $U_{o,bulk}$ = 2.30 V, which is expectedly a consequence of the size of the supercell.

All pathways involving a purely thermochemical step for $O_2$ ab/desorption are found to be inactive, due to high overpotential for the electrochemical steps (> 1.0 V).

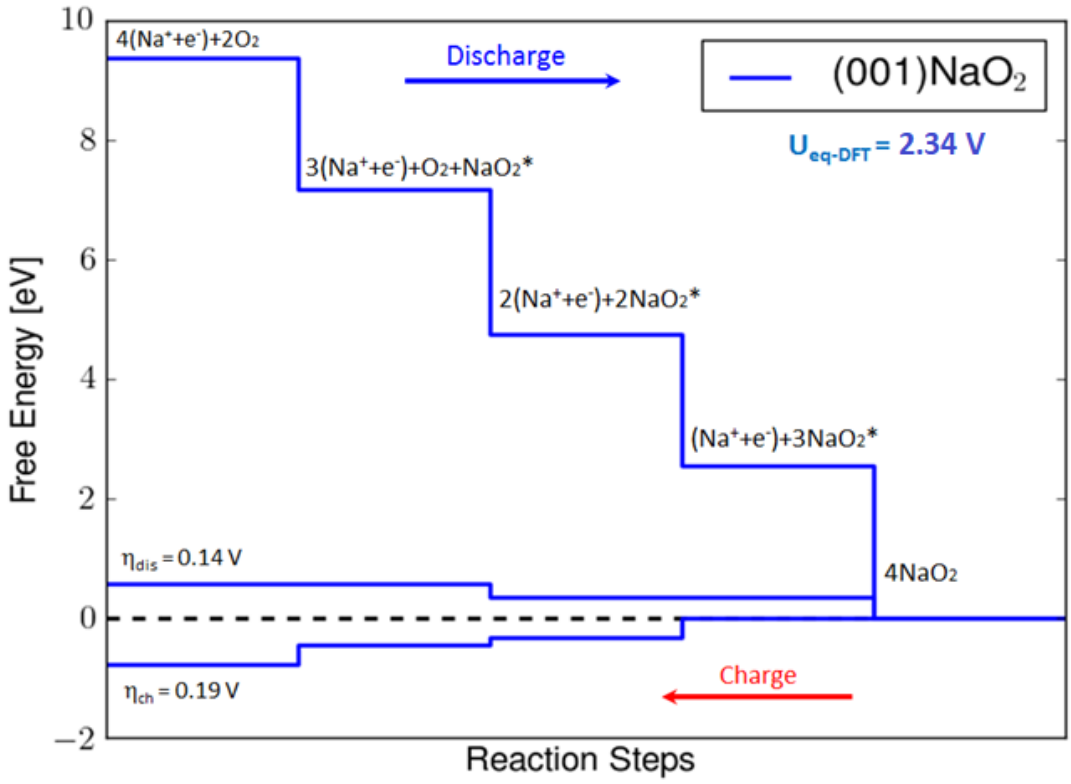


Figure 4: The calculated free energy diagram for $NaO_2$ growth/desorption mechanisms on stepped (001) $NaO_2$ surface.

### 3.3. $Na_2O_2$ Growth/Depletion Mechanisms on Front and Back Stepped $(1\bar{1}00)$ Surfaces

The $Na_2O_2$ discharge and charge pathways are studied on double stepped (front and back) $(1\bar{1}00)$ $Na_2O_2$ surface. Several pathways consisting of both chemical and electrochemical species have been investigated. As illustrated in Figure 5 and 6, the preferred growth (depletion) mechanism is found to be the path that has four electrochemical species, i.e. either Na* or $NaO_2$*, adsorbed to the step surface successively to grow (deplete) two formula units of $Na_2O_2$. This path becomes possible at minimum discharge (charge) overpotential of $\eta_{dis} = 0.69$ V ($\eta_{cha} = 0.68$ V). The first step is adsorption of $NaO_2$* species (Figure 5a) with a binding energy of 3.06 eV, which is the potential limiting step for the charge process and followed by the addition of $NaO_2$* (Figure 5b) with a binding energy of 2.98 eV. The last two steps are additions of two Na* species consecutively, with binding energies of 1.78 eV and 1.68 eV (the last step is the potential limiting step for discharge), as shown in Figures 5c and 5d. The full growth mechanism is accomplished with the growth of two formula units of $Na_2O_2$ at the step surface with an equilibrium potential of $U_0 = 2.37$ V. The calculated equilibrium potential is here in agreement with that calculated for bulk $Na_2O_2$. The charging process follows the same reaction steps as the discharge but in reverse order (from d to a in Figure 5 and

right to left in Figure 6). All pathways involving a purely thermochemical step are found to be inactive due to high overpotential for the electrochemical steps (> 1.5 V). The identified growth mechanism is similar to the one previously reported for $Li_2O_2$, [9,44] but the fundamental overpotentials for charge/discharge of $Na_2O_2$ are found to be substantially higher than those for $Li_2O_2$.

We thus find the overpotentials for growth (depletion) of $Na_2O_2$ of 0.69 V (0.68 V) to be prohibitively large compared to the low overpotential mechanism on $NaO_2$ (0.14 V and 0.19 V) and this therefore effectively blocks the formation of the thermodynamically preferred $Na_2O_2$, explaining why $NaO_2$ is the primary discharge product at standard conditions, as observed experimentally.

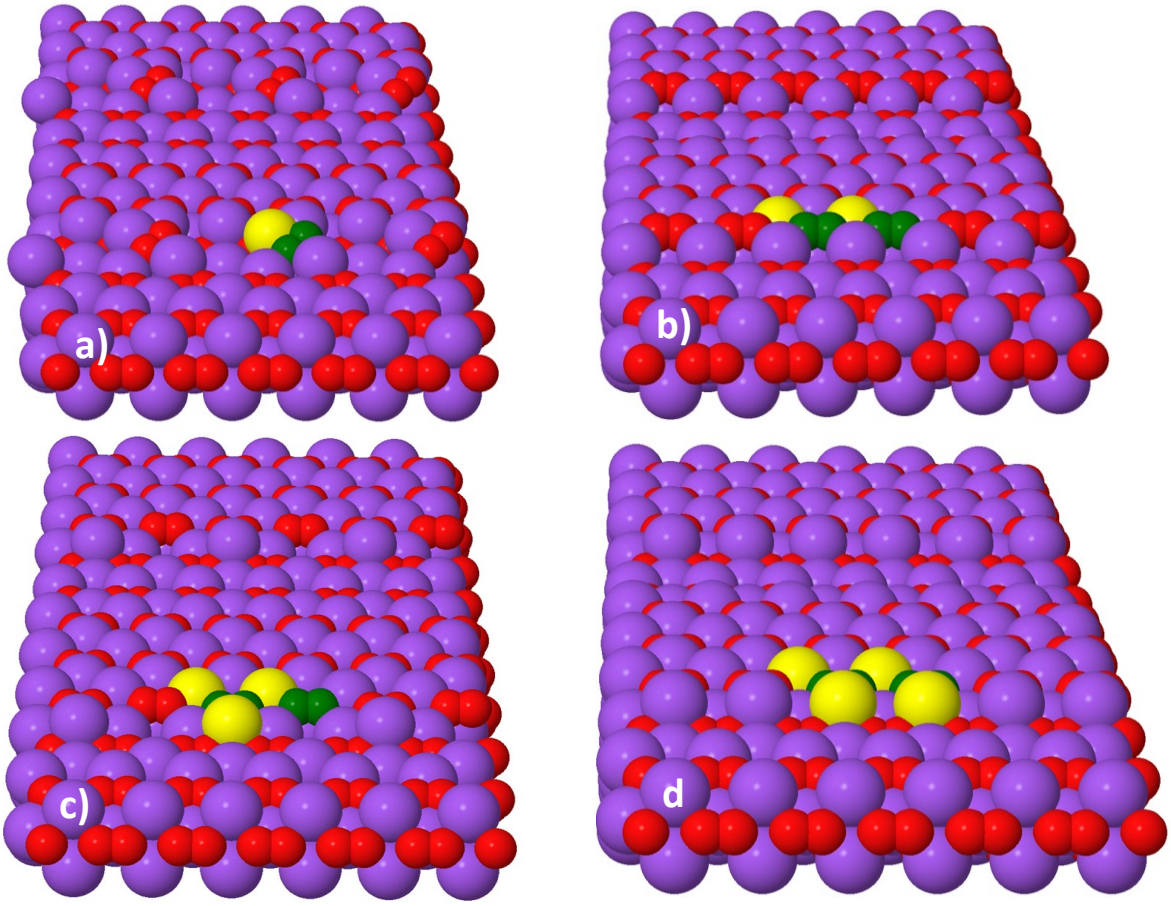


Figure 5: A four-step $Na_2O_2$ growth pathway on front and back stepped $Na_2O_2$ $(1\bar{1}00)$ surface during discharge. a) $NaO_2$, b) $NaO_2$, c) Na and d) Na consecutively adsorbs to the step surface to complete the growth of 2 formula units of $Na_2O_2$. Color: Na (purple) and O (red). Highlighted deposited ions: Na (yellow) and O (green).

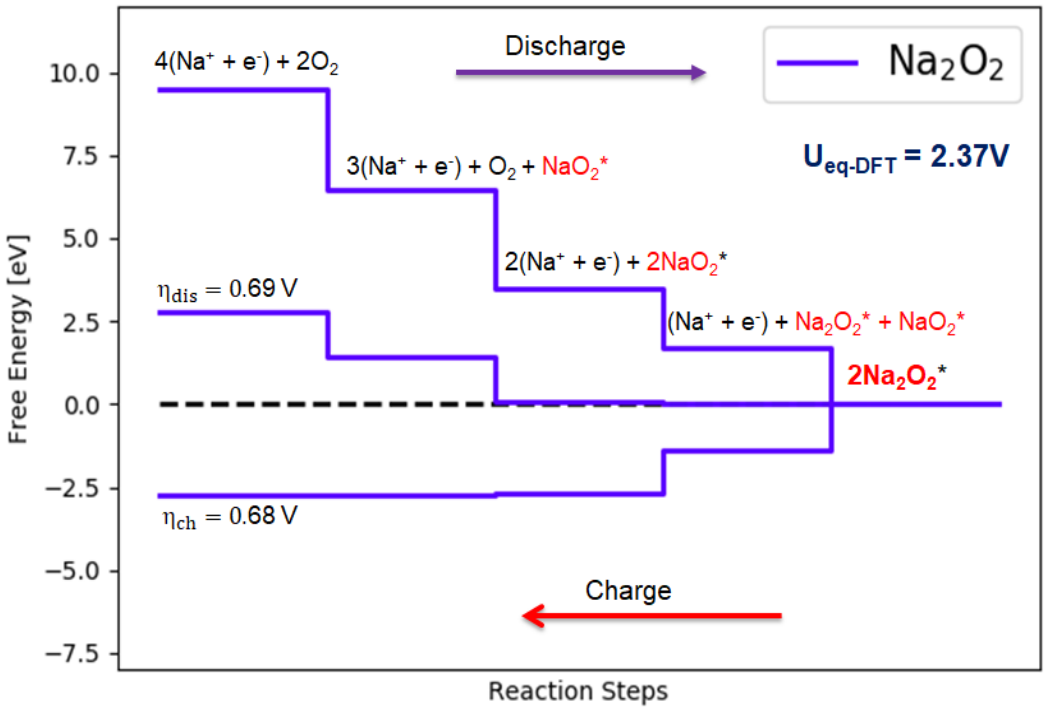


Figure 6: Calculated free energy diagrams for a four step $Na_2O_2$ growth mechanism on a stepped $(1\bar{1}00)$ $Na_2O_2$ surface, resulting in discharge (charge) overpotential of $\eta_{dis} = 0.69$ V ($\eta_{cha} = 0.68$ V).

### 3.4. Thermodynamics of Solution-Precipitation Mechanism

In the present work, the direct electrochemical crystal growth mechanism on stepped superoxide and peroxide surfaces, i.e. the so-called surface-based mechanism, has been thoroughly investigated using ab initio methods. However, it is important to note that for most electrolytes in Na-$O_2$ batteries, the solution-based mechanism dominates over the surface-based mechanism.[23,24,33,47,48] Although, to the best of our knowledge, the solvating energy of $NaO_2$, $\Delta G^{sol}_{NaO_2}$, has not been experimentally measured, it is possible to approximate it from the experimental solvating energies of $LiO_2$, $\Delta G^{sol}_{LiO_2}$, estimated by Johnson et al. [49] and the DFT dissolution energies of $NaO_2$ and $LiO_2$, calculated by Kim et al. [50]

Kim et al. calculated that the dissolution energy of $NaO_2$ is ~0.9 eV lower than that of $LiO_2$, while in the four solvents studied by Johnson et al., $\Delta G^{sol}_{LiO_2}$ spans from +0.37 eV for acetonitrile to -0.27 eV for 1-methylimidazole (a negative sign implies that the solution-based mechanism is preferred over the surface-based mechanism). Assuming that the difference in dissolution energies can be rigidly translated to the solvating energies (this is a very rough approximation), we infer that the solution-based mechanism is highly preferred in Na-$O_2$ batteries (from 0.5 eV/f.u. for acetonitrile to 1.2 eV/f.u. in 1-methylimidazole).

Since the disproportionation reaction of superoxide species formed in solution, i.e. 2 $NaO_2$ -> $Na_2O_2$ + $O_2$, will depend on the donor and acceptor number of the electrolyte [51], the formation of $Na_2O_2$ from the solution based mechanism would be suppressed in traditional high donor number electrolytes like DME and DMSO, pushing the product distribution further towards $NaO_2$ formation.

## IV. CONCLUSIONS

The free energy as a function of temperature for different phases of $NaO_2$ and $Na_2O_2$, as well as the dis/charge mechanisms on selected stepped surfaces have been investigated computationally using DFT calculations. Using a new metal chloride reference scheme, which accounts for the change in the oxidation state of the metal atoms, and a simple approximation to the entropic contributions, it is possible to describe the free energies of formation as a function of temperature for $NaO_2$ and $Na_2O_2$ in good agreement with experimental data. The experimentally found reaction product at room temperature, i.e. $NaO_2$, is slightly less thermodynamically stable than the expected $Na_2O_2$ product, but we show that the formation and depletion of $Na_2O_2$ is limited by large discharge and charge overpotentials of $\eta_{dis}$= 0.69 V and $\eta_{cha}$= 0.68 V, respectively. In contrast, the overpotentials for formation and dissolution of $NaO_2$ are small ($\eta_{dis}$= 0.14 V and $\eta_{cha}$= 0.19 V). The large difference in overpotentials, compared to the small difference of 0.10 eV in equilibrium potential can explain how epitaxial growth during discharge of a Na–$O_2$ battery results in the formation of $NaO_2$ as a dominant discharge product over the thermodynamically more stable $Na_2O_2$ in non-aqueous Na–$O_2$ batteries as observed in experiments.

## Acknowledgements

The authors acknowledge support of this work from the ReLiable project (Project No. 11-116792) funded by the Danish Council for Strategic Research Programme Commission on Sustainable Energy and Environment. Y.S.M. would like to acknowledge support from Addis Ababa University Thematic Research Project (Grant No. TR/012/2016). J.M.G.-L. acknowledges support from the Spanish Ministry of Economy and Competitiveness under projects FIS2012-30996 and FIS2010-21282-C02-01 and from the Mat4Bat project founded by Villum Foundation Young Investigators Program (Project No.10096).

## References


(1) Linden, D.; Reddy, T. B. *HANDBOOK OF BATTERIES*, Third Edit.; McGraw-Hill, 2001.

(2) Højberg, J.; McCloskey, B. D.; Hjelm, J.; Vegge, T.; Johansen, K.; Norby, P.; Luntz, A. C. An Electrochemical Impedance Spectroscopy Investigation of the Overpotentials in Li-$O_2$ Batteries. *ACS Appl. Mater. Interfaces* **2015**, *7*, 4039–4047.

(3) Lysgaard, S.; Christensen, M. K.; Hansen, H. A.; Maria, J.; Lastra, G.; Norby, P.; Vegge, T. Combined DFT and Differential Electrochemical Mass Spectrometry Investigation of the Effect of Dopants in Secondary Zinc – Air Batteries. *ChemSusChem* **2018**, *11*, 1–10.

(4) Tripkovic, V.; Hansen, H. A.; Vegge, T. Computational Screening of Doped Alpha-$MnO_2$ Catalysts for the Oxygen Evolution Reaction. *ChemSusChem* **2018**, *11*, 1–10.

(5) Mekonnen, Y. S.; Garcia-Lastra, J. M.; Hummelshøj, J. S.; Jin, C.; Vegge, T. Role of $Li_2O_2$@$Li_2CO_3$ Interfaces on Charge Transport in Non-Aqueous Li-Air Batteries. *J. Phys. Chem. C* **2015**, *119*, 18066–18073.

(6) McCloskey, B. D.; Speidel, A.; Scheffler, R.; Miller, D. C.; Viswanathan, V.; Hummelshøj, J. S.; Nørskov, J. K.; Luntz, A. C. Twin Problems of Interfacial Carbonate Formation in Nonaqueous Li-$O_2$ Batteries. *J. Phys. Chem. Lett.* **2012**, *3*, 997–1001.

(7) Younesi, R.; Norby, P.; Vegge, T. A New Look at the Stability of Dimethyl Sulfoxide and Acetonitrile in Li-$O_2$ Batteries. *ECS Electrochem. Lett.* **2014**, *3*, A15–A18.

(8) Younesi, R.; Veith, G. M.; Johansson, P.; Edström, K.; Vegge, T. Lithium Salts for Advanced Lithium Batteries: Li–metal, Li–$O_2$, and Li–S. *Energy Environ. Sci.* **2015**, *8*, 1905–1922.

(9) Mekonnen, Y. S.; Knudsen, K. B.; Mýrdal, J. S. G.; Younesi, R.; Højberg, J.; Hjelm, J.; Norby, P.; Vegge, T. Communication: The Influence of $CO_2$ Poisoning on Overvoltages and Discharge Capacity in Non-Aqueous Li-Air Batteries. *J. Chem. Phys.* **2014**, *140*, 121101.

(10) Luntz, A. C.; Mccloskey, B. D.; Dupré, N.; Cuisinier, M.; Guyomard, D. Nonaqueous Li − Air Batteries : A Status Report. *Interface* **2014**, *114*, 61–67.

(11) Xu, S.; Lau, S.; Archer, L. A. $CO_2$ and Ambient Air in Metal-Oxygen Batteries: Steps towards Reality. *Inorg. Chem. Front.* **2015**, *2*, 1070–1079.

(12) Balaish, M.; Kraytsberg, A.; Ein-Eli, Y. A Critical Review on Lithium-Air Battery Electrolytes. *Phys. Chem. Chem. Phys.* **2014**, *16*, 2801–2822.

(13) Armand, M.; Tarascon, J.-M. Building Better Batteries. *Nature* **2008**, *451*, 652–657.

(14) Aurbach, D.; McCloskey, B. D.; Nazar, L. F.; Bruce, P. G. Advances in Understanding Mechanisms Underpinning Lithium-Air Batteries. *Nat. Energy* **2016**, *1*, 1–11.

(15) Vegge, T.; Garcia-Lastra, J. M.; Siegel, D. J. Lithium–Oxygen Batteries: At a Crossroads? *Curr. Opin. Electrochem.* **2017**, *6*, 100–107.

(16) Das, S. K.; Lau, S.; Archer, L. a. Sodium–oxygen Batteries: A New Class of Metal–air Batteries. *J. Mater. Chem. A* **2014**, *2*, 12623–12629.

(17) Hartmann, P.; Bender, C. L.; Vračar, M.; Dürr, A. K.; Garsuch, A.; Janek, J.; Adelhelm, P. A Rechargeable Room-Temperature Sodium Superoxide ($NaO_2$) Battery. *Nat. Mater.* **2013**, *12*, 228–232.

(18) Zhao, N.; Li, C.; Guo, X. Long-Life Na-$O_2$ Batteries with High Energy Efficiency Enabled by Electrochemically Splitting $NaO_2$ at a Low Overpotential. *Phys. Chem. Chem. Phys.* **2014**, *16*, 15646–15652.

(19) Bender, C. L.; Hartmann, P.; Vračar, M.; Adelhelm, P.; Janek, J. On the Thermodynamics, the Role of the Carbon Cathode, and the Cycle Life of the Sodium Superoxide ($NaO_2$) Battery. *Adv. Energy Mater.* **2014**, *4*, 2–11.

(20) Knudsen, K. B.; Nichols, J. E.; Vegge, T.; Luntz, A. C.; Mccloskey, B. D.; Hjelm, J. An Electrochemical Impedance Study of the Capacity Limitations in Na−$O_2$ Cells. *J. Phys. Chem. C* **2016**, *120*, 10799–10805.

(21) Kim, J.; Lim, H.-D.; Gwon, H.; Kang, K. Sodium–oxygen Batteries with Alkyl-Carbonate and Ether Based Electrolytes. *Phys. Chem. Chem. Phys.* **2013**, *15*, 3623–3629.

(22) Hartmann, P.; Bender, C. L.; Sann, J.; Dürr, A. K.; Jansen, M.; Janek, J.; Adelhelm, P. A Comprehensive Study on the Cell Chemistry of the Sodium Superoxide ($NaO_2$) Battery. *Phys. Chem. Chem. Phys.* **2013**, *15*, 11661–11672.

(23) Mccloskey, B. D.; Garcia, J. M.; Luntz, A. C. Chemical and Electrochemical Differences in Nonaqueous Li−$O_2$ and Na−$O_2$ Batteries. *J. Phys. Chem. Lett.* **2014**, *5*, 1230–1235.

(24) Lutz, L.; Yin, W.; Grimaud, A.; Corte, D. A. D.; Tang, M.; Johnson, L.; Azaceta, E.; Naylor, A. J.; Hamad, S.; Anta, J. A.; et al. High Capacity Na−$O_2$ Batteries: Key Parameters for Solution- Mediated Discharge. *J. Phys. Chem. C* **2016**, *120*, 20068–20076.

(25) Li, Y.; Yadegari, H.; Li, X.; Banis, M. N.; Li, R.; Sun, X. Superior Catalytic Activity of Nitrogen-Doped Graphene Cathodes for High Energy Capacity Sodium-Air Batteries. *Chem.*

*Commun. (Camb).* **2013**, *49*, 11731–11733.

(26) Liu, W.; Sun, Q.; Yang, Y.; Xie, J.-Y.; Fu, Z.-W. An Enhanced Electrochemical Performance of a Sodium–air Battery with Graphene Nanosheets as Air Electrode Catalysts. *Chem. Commun.* **2013**, *49*, 1951–1953.

(27) Hu, Y.; Han, X.; Zhao, Q.; Du, J.; Cheng, F.; Chen, J. Porous Perovskite Calcium-Manganese Oxide Microspheres as Efficient Catalyst for Rechargeable Sodium-Oxygen Batteries. *J. Mater. Chem. A* **2015**, *3*, 3320–3324.

(28) Yang, S.; Siegel, D. J. Intrinsic Conductivity in Sodium-Air Battery Discharge Phases: Sodium Superoxide vs Sodium Peroxide. *Chem. Mater.* **2015**, *27*, 3852–3860.

(29) He, M.; Lau, K. C.; Ren, X.; Xiao, N.; Mcculloch, W. D.; Curtiss, L. A.; Wu, Y. Concentrated Electrolyte for the Sodium–Oxygen Battery:Solvation Structure and ImprovedCycle Life. *Angew. Chem.* **2016**, *128*, 15536–15540.

(30) Bender, C. L.; Schrçder, D.; Pinedo, R.; Adelhelm, P.; Janek, J. One- or Two-Electron Transfer ? The Ambiguous Nature of the Discharge Products in Sodium – Oxygen Batteries Minireviews. *Angew. Chemie - Int. Ed.* **2016**, *55*, 4640–4649.

(31) Kang, S.; Mo, Y.; Ong, S. P.; Ceder, G. Nanoscale Stabilization of Sodium Oxides: Implications for Na-O2 Batteries. *Nano Lett.* **2014**, *14*, 1016–1020.

(32) Ortiz-Vitoriano, N.; Batcho, T. P.; Kwabi, D. G.; Han, B.; Pour, N.; Yao, K. P. C.; Thompson, C. V.; Shao-Horn, Y. Rate-Dependent Nucleation and Growth of $NaO_2$ in Na–$O_2$ Batteries. *J. Phys. Chem. Lett.* **2015**, *6*, 2636–2643.

(33) Hartmann, P.; Heinemann, M.; Bender, C. L.; Graf, K.; Baumann, R. P.; Adelhelm, P.; Heiliger, C.; Janek, J. Discharge and Charge Reaction Paths in Sodium-Oxygen Batteries: Does $NaO_2$ Form by Direct Electrochemical Growth or by Precipitation from Solution? *J. Phys. Chem. C* **2015**, *119*, 22778–22786.

(34) Hummelshøj, J. S.; Luntz, A. C.; Nørskov, J. K. Theoretical Evidence for Low Kinetic Overpotentials in Li-$O_2$ Electrochemistry. *J. Chem. Phys.* **2013**, *138*, 034703.

(35) Christensen, R.; Hummelshøj, J. S.; Hansen, H. A.; Vegge, T. Reducing Systematic Errors in Oxide Species with Density Functional Theory Calculations. *J. Phys. Chem. C* **2015**, *119*, 17596–17601.

(36) Perdew, J. P.; Burke, K.; Ernzerhof, M. Generalized Gradient Approximation Made Simple. *Phys. Rev. Lett.* **1996**, *77*, 3865–3868.

(37) Enkovaara, J.; Rostgaard, C.; Mortensen, J. J.; Chen, J.; Dułak, M.; Ferrighi, L.; Gavnholt, J.; Glinsvad, C.; Haikola, V.; Hansen, H. a; et al. Electronic Structure Calculations with GPAW: A Real-Space Implementation of the Projector Augmented-Wave Method. *J. Phys. Condens. Matter* **2010**, *22*, 253202.

(38) Bahn, S. R.; Jaconsen, K. W. An Object-Oriented Scripting Interface to a Legacy Electronic Strcture Code. *Comput. Sci. Eng.* **2002**, *4*, 56–66.

(39) Blochl, P. E. Projected Augmented-Wave Method. *Phys. Rev. B* **1994**, *50*, 17953–17979.

(40) Mortensen, J. J.; Hansen, L. B.; Jacobsen, K. W. A Real-Space Grid Implementation of the Projector Augmented Wave Method. *Phys. Rev. B* **2005**, *71*, 035109.

(41) Radin, M. D.; Rodriguez, J. F.; Tian, F.; Siegel, D. J. Lithium Peroxide Surfaces Are Metallic, While Lithium Oxide Surfaces Are Not. *J. Am. Chem. Soc.* **2012**, *134*, 1093–1103.

(42) Radin, M.; Rodriguez, J.; Siegel, D. Lithium Peroxide Surfaces and Point Defects: Relevance for Li-Air Batteries. *Proc. Batter. Congr.* **2011**, *6*, 1–6.

(43) Mýrdal, J. S. G.; Vegge, T. Selective Poisoning of Li–air Batteries for Increased Discharge Capacity. *RSC Adv.* **2014**, *4*, 15671–15674.

(44) Hummelshøj, J. S.; Blomqvist, J.; Datta, S.; Vegge, T.; Rossmeisl, J.; Thygesen, K. S.; Luntz, A. C.; Jacobsen, K. W.; Nørskov, J. K. Communications: Elementary Oxygen Electrode Reactions in the Aprotic Li-Air Battery. *J. Chem. Phys.* **2010**, *132*, 130–133.

(45) Nørskov, J. K.; Rossmeisl, J.; Logadottir, A.; Lindqvist, L.; Lyngby, D.-; Jo, H. Origin of the Overpotential for Oxygen Reduction at a Fuel-Cell Cathode. *J. Phys. Chem. B* **2004**, *108*, 17886–17892.

(46) Chase, M. W. NIST-JANAF Thermochemical Tables. *American Chemical Society; American Institute of Physics for the National Institute of Standards and Technology: Washington, DC.* 1998.

(47) Radin, M. D.; Siegel, D. J. Charge Transport in Lithium Peroxide: Relevance for Rechargeable Metal–air Batteries. *Energy Environ. Sci.* **2013**, *6*, 2370–2379.

(48) Liu, T.; Kim, G.; Casford, M. T. L.; Grey, C. P. Mechanistic Insights into the Challenges of Cycling a Nonaqueous Na−$O_2$ Battery. *J. Phys. Chem. Lett.* **2016**, *7*, 4841–4846.

(49) Johnson, L.; Li, C.; Liu, Z.; Chen, Y.; Freunberger, S. A.; Ashok, P. C.; Praveen, B. B.; Dholakia, K.; Tarascon, J.; Bruce, P. G. The Role of $LiO_2$ Solubility in $O_2$ Reduction in Aprotic Solvents and Its Consequences for Li–O2 Batteries. *Nat. Chem.* **2014**, *6*, 1091–

1099.

(50) Kim, J.; Park, H.; Lee, B.; Seong, W. M.; Lim, H.; Bae, Y.; Kim, H.; Kim, W. K.; Ryu, K. H.; Kang, K. Dissolution and Ionization of Sodium Superoxide in Sodium–oxygen Batteries. *Nat. Commun.* **2016**, *7*, 10670.

(51) Li, O.; Aetukuri, N. B.; Mccloskey, B. D.; García, J. M.; Krupp, L. E.; Viswanathan, V.; Luntz, A. C. Solvating Additives Drive Solution-Mediated Electrochemistry and Enhance Toroid Growth in Non-Aqueous Li-$O_2$ Batteries. *Nat. Chem.* **2015**, *7*, 50–56.